Effects of Charged Amino Acid Mutations on the Bimolecular Kinetics of Reduction of Yeast Iso-1-ferricytochrome *c* by Bovine Ferrocytochrome b_5†

Scott H. Northrup,* Kathryn A. Thomasson, and Cynthia M. Miller

Department of Chemistry, Tennessee Technological University, Cookeville, Tennessee 38505

Paul D. Barker,‡ Lindsay D. Eltis,§ J. Guy Guillemette, Stephen C. Inglis, and A. Grant Mauk*

Department of Biochemistry, University of British Columbia, Vancouver, British Columbia, Canada, V6T 1Z3

Received December 9, 1992; Revised Manuscript Received March 18, 1993

ABSTRACT: The reduction of wild-type yeast iso-1-ferricytochrome *c* (ycytc) and several mutants by trypsin-solubilized bovine liver ferrocytochrome b_5 (cytb5) has been studied under conditions in which the electron-transfer reaction is bimolecular. The effect of electrostatic charge modifications and steric changes on the kinetics has been determined by experimental and theoretical observations of the electron-transfer rates of ycytc mutants K79A, K′72A, K79A/K′72A, and R38A (K′ is used to signify trimethyllysine (Tml)). A structurally robust Brownian dynamics (BD) method simulating diffusional docking and electron transfer was employed to predict the mutation effect on the rate constants. A realistic model of the electron-transfer event embodied in an intrinsic unimolecular rate constant is used which varies exponentially with donor–acceptor distance. The BD method quantitatively predicts rate constants over a considerable range of ionic strengths. Semiquantitative agreement is obtained in predicting the perturbing influence of the mutations on the rate constants. Both the experimentally observed rate constants and those predicted by BD descend in the following order: native ycytc > K79A > K′72A > K79A/K′72A. Variant R38A was studied at a different ionic strength than this series of mutations, and the theory agreed with experiment in predicting a smaller rate constant for the mutant. In all cases the predicted effect of mutation was in the correct direction, but not as large as that observed. The BD simulations predict that the two proteins dock through essentially a single domain, with a distance of closest approach of the two heme groups in rigid body docking typically around 12 Å. Two predominant classes of complexes were calculated, the most frequent involving the quartet of cytb5/ycytc interactions, Glu48–Arg13, Glu56–Lys87, Asp60–Lys86, and heme–Tml72, having an average electrostatic energy of −13.0 kcal/mol. The second most important complexes were of the type previously postulated (Salemme, 1976; Mauk et al., 1986; Rodgers et al., 1988) with interactions Glu44–Lys27, Glu48–Arg13, Asp60–Tml72, and heme–Lys79 and having an energy of −6.4 kcal/mol. The ionic strength dependence of the bimolecular reaction rate was well reproduced using a discontinuous dielectric model, but poorly so for a uniform dielectric model.

The quantification of physical and chemical factors that determine electron-transfer rates between cytochromes is a topic of considerable interest (Marcus & Sutin, 1985; King et al., 1985; Gray, 1986; Northrup et al., 1988, 1990; Mayo et al., 1986; Hoffman & Ratner, 1987; Hazzard et al., 1987; Summers & Erman, 1988; Wendoloski et al., 1987; Dixon et al., 1989, 1990). The reduction of yeast iso-1-ferricytochrome *c* (ycytc) by trypsin-solubilized ferrocytochrome b_5 (cytb5) is an attractive prototypical system for the study of such factors, in that these proteins are small, soluble, structurally well-characterized (Bushnell et al., 1990; Mathews et al., 1972, 1986), and readily modified by site-directed mutagenesis (Pielak et al., 1985; von Bodman et al., 1986; Funk et al., 1990). We recently studied this reaction (using the native horse heart ferricytochrome *c* (hcytc)) as a function of pH, temperature, and ionic strength to gain greater insight into the structural and functional properties that determine the rate of electron transfer under second-order reaction conditions (Eltis, et al., 1991). We demonstrated that one can make semiquantitative predictions of ionic strength and pH dependence on this system using the Brownian dynamics (BD) simulation method and a dipolar sphere model of the proteins (Northrup et al., 1986, 1990). Using that simple theory, we provided an interpretative framework for understanding the role of electrostatics, ionic strength, temperature and pH effects, and geometric reactive criteria in the bimolecular rates observed in the experiments. However, a simple three-charge model is expected to fail when used to predict the detailed effects of point mutations involving charged amino acid residues.

In this present study, we have evaluated the effect of electrostatic charge modifications and steric changes on the bimolecular kinetics of the reduction of ycytc by cytb5 by experimental and theoretical observations of the electron-transfer rates of ycytc mutants K79A, K′72A, K79A/K′72A, and R38A (K′ or Tml denotes trimethyllysine). Tml72 and Lys79 are two key charged residues near the heme crevice which are involved in ionic contacts with cytochrome partners, while Arg38 lies outside of the heme-exposed face. Here we

† This work has been made possible by Grants GM34248 (S.H.N.) and GM33804 (A.G.M.) from the National Institutes of Health, by Grant MT1706 from the Medical Research Council of Canada (to Michael Smith), by Grant 24159-B6 (S.H.N.) from the Petroleum Research Fund as administered by the American Chemical Society, and by the Camille and Henry Dreyfus Scholar/Fellow Program for Undergraduate Institutions (at TTU). S.H.N. is a Camille and Henry Dreyfus Scholar; K.A.T. is a Camille and Henry Dreyfus Fellow.

* Authors to whom correspondence should be addressed.

‡ Present address: Cambridge Centre for Protein Engineering, Medical Research Council Centre, Hills Road, Cambridge CB2 2QH, U.K.

§ Present address: Gesellschaft Biotechnologisch Forschung, Mascherode-r Weg 12, D-3330 Braunschweig, Germany.

0006-2960/93/0432-6613$04.00/0

put to the test the most rigorous BD simulation technique available to determine whether the effect of mutation of these charged residues can be predicted by the simulation theory.

EXPERIMENTAL METHODS

Glass-distilled water purified with a Barnstead NANOpure system to a resistivity of 16–17 MΩ was used in all experimental work. All pH measurements were performed with a Radiometer Model PHM 84 pH meter that was equipped with a Radiometer Type GK 2321C combination electrode. Except where noted, reagent-grade chemicals were used. Phosphate buffers of specified pH and ionic strength were prepared from monobasic and dibasic sodium salts purchased from BDH Chemical Co.

Protein Preparation. The tryptic fragment of bovine hepatic cytochrome b_5 was prepared as previously described (Reid & Mauk, 1982). The generation and purification of variant forms of yeast iso-1-cytochrome *c* from *Saccharomyces cerevisiae* have also been described previously (Pielak et al., 1985; Cutler et al., 1989; Inglis et al., 1991; Rafferty et al., 1991). All cytochromes *c* possessed an additional substitution at position 102 in which the naturally occurring cysteinyl residue was replaced with a threonyl residue to prevent intermolecular disulfide bond formation and to decrease the rate of ferricytochrome *c* autoreduction (Cutler et al., 1987). Protein solutions were concentrated by centrifugal ultrafiltration using Centripreps and Centricons (Amicon). Protein concentrations were determined on the basis of $\epsilon_{409.5} = 106.1\ mM^{-1}$ and $\epsilon_{412.5} = 117.0\ mM^{-1}$ for cytochrome *c* (Margoliash & Frohwirt, 1959) and cytochrome b_5 (Ozols & Strittmatter, 1964), respectively.

Stopped-Flow Kinetics. Rapid mixing experiments were performed with a stopped-flow spectrophotometer installed in a glove box (Vacuum Atmospheres) as described previously (Eltis, 1989; Leung et al., 1989). The data acquisition and instrument control signals were collected and manipulated with a microcomputer (OLIS, Bogart, GA). The reduction of ferricytochrome *c* by ferrocytochrome b_5 was performed under second-order conditions with the reactants at equimolar concentrations (~1.7 μM). Ammonium bis(dipicolinato)-cobaltate(III) was used to assure quantitative conversion to ferricytochrome *c* (Mauk et al., 1979). Ferricytochrome b_5 was reduced to the ferrocytochrome by steady-state illumination in the presence of 0.05 equiv of lumiflavin (Eltis et al., 1990).

Oxidation of ferrocytochrome b_5 was monitored at 428 nm, an isosbestic point for ferri-/ferrocytochrome *c*. The reduction of ferricytochrome *c* was monitored at 416 nm, an isostestic point in the electronic absorption spectra of ferri- and ferrocytochrome b_5 (Eltis et al., 1990). A minimum of five decay curves was averaged for each measurement, unless the half-life of the reaction exceeded 2 min; in this case two or three decay curves were averaged. The data were fit to a rate equation using the nonlinear least-squares fitting program MINSQ (ver. 3) (MicroMath Scientific Software, Salt Lake City, UT).

Monophasic data were fit to a second-order rate equation:

$$A_t = \frac{A_0 - A_\infty}{1 + kc_0 t} \tag{1}$$

in which the initial concentrations, c_0 of the cytochromes are equal. In this equation, A_t is the absorbance at time t, A_0 and A_∞ are the initial and final absorbances of the protein solution, respectively, and k is the second-order rate constant. At lower ionic strengths, the initial portion of the reaction occurred within the dead time of the instrument. In these cases, the initial concentration of the cytochromes was determined by normalizing the overall change of absorbance (A_{tot}) to A_{tot} observed for the reaction performed at high ionic strength. Biphasic data were split into two data sets. The first half of the data set was fit to a second-order equation in which the initial concentrations of the cytochromes were not equal:

$$A_t = \frac{(c_0 - b_0) - A_0 + c_0(e^{c_0 - b_0 k_t} - 1)A_I}{c_0 e^{c_0 - b_0 k_t} - b_0} \tag{2}$$

The initial concentration, c_0, of ferricytochrome *c* was determined by

$$c_0 = b_0 \frac{(A_{MAX} - A_\infty)}{A_{MAX}} \tag{3}$$

The second half of the biphasic data sets was fit to a first-order rate equation:

$$A_t = (A_0 - A_\infty)e^{k_1 t} + A_\infty \tag{4}$$

The second-order rate constant for ferrocytochrome b_5 reduction of R38A was studied at an ionic strength of 0.163 M sodium phosphate buffer (pH 7.0, 25 °C). Ferrocytochrome b_5 reduction of K'72A and K79A ferricytochrome *c* variants was studied over an ionic strength range of 0.1–1.5 M (pH 7.0, 25 °C).

THEORETICAL METHODS

Charge Assignments. The starting point of our atomic-scale modeling of these proteins was the X-ray crystallographic coordinates for ycytc of Brayer and co-workers (Louie et al., 1990) and cytb5 (Mathews et al., 1972, 1986). The structure of the yeast ferricytochrome was assumed for our purposes to be similar to the reduced form available in the data bank (Bernstein et al., 1977). The protonation state of each titratable amino acid residue was estimated by performing a Tanford–Kirkwood calculation with the static-accessibility modification (Matthew, 1985; Tanford & Kirkwood, 1957; Tanford & Roxby, 1972; Shire et al., 1974). Thus, each residue was assigned a net charge based on its protein environment, pH, ionic strength, and temperature. At or near neutral pH, as in these studies, lysines and arginines are fully protonated and carboxylates are fully dissociated. The more ambiguous assignments of charge of amino terminii and histidines depend on environmental parameters and were estimated by the Tanford–Kirkwood calculation. The fractional net charge calculated for histidines was incremented onto the charge at either the $N_{\delta 1}$ or $N_{\epsilon 2}$ atom, whichever led to greater overall stability of the protein. Partial charges were assigned to all other atoms from the set used previously (Northrup et al., 1981). Table I gives the protonation status of titratable sites produced by this method for the native species.

The modeling of site-specific mutations was performed by substituting the side-chain coordinates of the lysines and arginine by the standard residue side-chain coordinates of the alanines directly into the initial crystallographic structures with no further refinements.

Brownian Dynamics Method. The basic BD method as we have applied it to reactions between two whole translating and rotating proteins has already been described in previous publications (Northrup et al., 1984, 1987a,b, 1988, 1990), so we simply provide an overview. In BD, the Brownian motion of two interacting proteins in a solvent is simulated by a series of small displacements governed by the Smoluchowski diffusion equation with forces. The Ermak and McCammon (1978)

Table I: Charge Assignments Predicted by the Tanford–Kirkwood Algorithm with Static-Accessibility Modification at pH 7.0, T = 25° C, and $I = 0.19m$[a]

ferrocytochrome b_5		yeast iso-1-ferricytochrome c	
residue	assigned charge	residue	assigned charge
N-terminal residue	0.98	N-terminal residue	0.96
His15	0.24	His26	0.15
His26	0.29	His39	0.20
His80	0.34	lysines	1.00
lysines	1.00	arginines	1.00
arginines	1.00	glutamates	−1.00
glutamates	−1.00	aspartates	−1.00
aspartates	−1.00	carboxy terminal	−1.00
carboxy terminal	−1.00	heme propionates	−1.00
heme propionates	−1.00		
total charge	−8.15	total charge	+7.31

[a] Protein radii are assumed to be 15.9 and 16.6 Å for cytb5 and ycytc, respectively. Protein exclusion surface is 2.0 Å larger than the protein radii. Interior dielectric is 4.0.

algorithm for free displacements, $\Delta\vec{r}$, in the relative separation vector, $\vec{r}$, of reactant centers of mass in a time step, Δt, is

$$\Delta\vec{r} = \frac{D\Delta t}{k_B T}\vec{F} + \vec{S} \tag{5}$$

Here D is the spatially isotropic translational diffusion coefficient for relative motion, $\vec{F}$ is the systematic interparticle (electrostatic) force, $k_B T$ is the Boltzmann constant multiplied by absolute temperature, and $\vec{S}$ is the stochastic component of the displacement arising from collisions of particles with solvent molecules and is generated by taking normally distributed random numbers obeying the average relationship $\langle S^2\rangle = 2D\Delta t$. A similar equation governs the independent rotational Brownian motion of each particle, where force is replaced by torque and D is replaced by an isotropic rotational diffusion coefficient for each protein.

The connection of BD trajectory statistics with bimolecular rate constants is made by separating the problem into the easy one of centrosymmetric diffusion to a starting surface b from the outside, followed by diffusion in a complicated force field inside b, where BD simulation provides the description. Trajectories of diffusing species are begun at random orientations from a separation $r = b$ = 65 Å, which is outside the region of asymmetric Coulombic forces, and are truncated at an outer spherical surface c = 200 Å. For reactions where the bimolecular rate constant is near 10^7 M^{-1} s^{-1}, on the order of 10 000 trajectories are required to obtain statistically significant values of the probability p of eventual association of pairs into favorable geometries for reaction prior to ultimate separation to distance $r = c$. The diffusion-controlled bimolecular reaction rate constant k may then be extracted from p by applying the formula

$$k = k_D(b)p\left[1 - (1-p)\frac{k_D(b)}{k_D(c)}\right]^{-1} \tag{6}$$

Here, the diffusive rate constant $k_D(s)$ for first arrival at spherical surface s is given by the Smoluchowski–Debye expression when centrosymmetric forces apply in the region $r > s$:

$$k_D(s) = \{\int_s^\infty dr\,[4\pi r^2 D(r)]^{-1} e^{u(r)/k_B T}\}^{-1} \tag{7}$$

where s is a starting or truncation surface radius, $D(r)$ is a spatially dependent relative translational diffusion coefficient, and $u(r)$ is a centrosymmetric potential energy of interaction between the diffusing pair.

We may study the influence of a whole range of different reaction boundary conditions simultaneously in a single simulation, monitoring the survival of the trajectory with respect to a parallel set of survival probabilities w_i, which correspond to a parallel set of reaction criteria i. The reaction probability p_i for reactive criterion i is then $p_i = 1 - w_i$.

The full rotational treatment of two irregularly shaped translating and rotating proteins was introduced in our recent work (Northrup & Herbert, 1990). In our BD scheme for reaction between two proteins, we typically choose one of the proteins of a reacting pair to be designated protein I, or the target protein. In these studies cytb5 is chosen as the target protein. All motion is monitored in the reference frame chosen to rotate and translate along with protein I. Thus, while rotations and translations of both proteins are computed, rotations of the first protein show up as translations of protein II in the reference frame fixed upon protein I. A more complete mathematical description of our treatment of rotations is presented by Allison and co-workers (Nambi et al., 1991).

To treat excluded volume interactions between proteins, a 71 × 71 × 71 element cubic spatial exclusion grid of 1.0-Å resolution is generated about protein I to define its excluded volume. A test atom is place at each grid point, and the distance to each of the atoms of protein I is determined. If the test atom falls within 2.7 Å of any atom in the protein, that grid point is defined to be in an excluded region. All surface atoms of protein II are tested against this grid after each Brownian step to check for atomic overlaps, and steps which violate the excluded region are repeated.

Electrostatic Forces. The electrostatic forces between proteins were treated by iterating the finite-difference numerical solution of the linearized Poisson-Boltzmann (LPB) equation on a cubic lattice by the Warwicker and Watson (1982) method as adapted by Klapper et al. (1986). The electrostatic potential field surrounding each isolated protein was computed, each represented as an irregularly shaped cavity of low dielectric constant ($\epsilon = 4$) and zero internal ionic strength and having fixed imbedded charges in the crystallographic configuration. Surrounding the protein cavity is a continuum dielectric with $\epsilon = 78.3$ representative of bulk water and having appropriate ionic strengths. We used the "focusing" method, in which we first iterated a solution on an outer lattice of dimension 51^3 elements having a resolution of 3 Å and encompassing a region of size $(150\text{ Å})^3$ centered on the protein. With such a large region, the outer boundary potential can be set to the primitive Coulomb–Debye result. Once a solution was obtained on this outer coarse grid, an additional calculation was performed on a refined grid of resolution of 1.0 Å. Trial solutions and boundary values for this inner lattice were constructed from the outer lattice solution.

The direct force between the two proteins and the torque operating on protein II (ycytc) were determined at each time step by placing the protein II array of test charges into the field around the protein I (cytb5) cavity and, consulting the stored grid of forces, performing a summation over all protein II charges. For a more accurate and self-consistent treatment of the interaction between two proteins, one would need to include an additional low dielectric cavity representing the protein II interior in the presence of the protein I cavity. However, one would need to iterate a solution for every possible mutual configuration of the two protein cavities. We instead have resorted to a simplification ignoring the low dielectric in the protein II interior as well as allowing the electrolyte screening effect to operate throughout its interior.

Rotation. The above procedure allows for treatment of the rotation of protein II in a field of torque generated by protein I. We also included the rotation of protein I in the field of protein II by consulting the inner and outer force lattice around protein II. These lattices rotate in rigid body rotation with protein II. A dipolar pair of charges was included on protein I to serve as test charges which interact with the field around protein II and was used to compute the approximate torque on protein I in the field of protein II. This feature of two rotating proteins is essential in treating protein pairs which are comparably sized.

Reaction Criteria. Two models have been constructed to embody the chemical reaction event. In the primitive *distance cutoff model*, reaction is assumed to occur instantaneously when the distance d between edges of the porphyrin rings reaches a prescribed value d_{rx} and the angle ψ between heme plane normals is less than a prescribed value ψ_{rx}. The distance d was computed as the shortest distance between any atom in the heme atom set (CHA, CHB, CHC, CHD) chosen to represent the periphery of the porphyrin system on protein I and the same set on protein II, minus a constant shift factor of 5 Å to account for the distance of closest approach of this set of atoms in a perfect edge-on arrangement.

A second model studied was the *exponential reactivity model*, originally employed in our study of self-exchange in *Pseudomonas aeruginosa* cytochrome c_{551} (Herbert & Northrup, 1989) and subsequently used in our treatment of the present reaction with the dipolar sphere model (Eltis et al., 1991) and in self-exchange reactions of other cytochromes (Andrew et al., 1993). This ideally provides a more physically realistic model of the electron-transfer event in which the intrinsic spatially dependent electron-transfer rate constant, $k_{et}(d)$, is given as a function of d by

$$k_{et}(d) = k_{et}^{\circ} \exp(-\beta d) \tag{8}$$

This roughly measures reactivity as a function of distance between the π systems of the two porphyrins. Here, preexponential factor, k_{et}°, is the electron-transfer rate constant when porphyrins are in direct contact edge-on and was calibrated in our study by matching theoretical to experimental bimolecular rate constants for the wild-type ycytc/cytb5 reaction at the lowest ionic strength $I = 0.19m$ and pH = 7. Values of k_{et}° are expected to be on the order of 10^{11} s^{-1}. Even faster electron-transfer rates would occur for porphyrins in a sandwich orientation at contact (Siders et al., 1984), but such orientations are excluded in cytochromes since the heme groups are generally perpendicular to the protein surface. The electron-transfer distance-dependent factor β is a quantity of intense interest (McLendon, 1988) and is adjustable in our study and varied to fit the experimental data. Thus, an estimate of this important factor can be obtained from BD. The intrinsic rate constant $k_{et}(d)$ was incorporated into BD as follows. The spatially dependent probability $\mathcal{P}(d)$ that the reactant pair will survive a given Brownian step Δt without electron transfer is $\mathcal{P}(d) = \exp(-k_{et}(d)\Delta t)$. This probability is multiplicative throughout the trajectory, finally giving the escape probability for that trajectory.

The appropriate reaction criteria parameters are unknown and were treated as adjustable parameters to be calibrated on the reaction of the native ycytc with cytb5 and then applied to the mutant proteins. In our simulations using the exponential reactivity model, we varied the value of the exponential decay parameter β from 1.0 to 1.2 Å^{-1} using a preexponential factor of $k_{et}^{\circ} = 10^{11}$ s^{-1}. This range of β was chosen to be consistent with values we found (Herbert & Northrup, 1989) to match theoretical results with experiment (Timkovich et al., 1988) in simulations of the self-exchange reaction of *P. aeruginosa* cytochrome c_{551}. For the distance cutoff model, we varied d_{rx} from 10.0 to 12.0 Å and ψ from 15.0° to 90.0°. This range of d_{rx} was found to place the proteins in contact with their heme peripheral atoms at a minimum sterically achievable distance.

Table II: Net Charge, Dipole Moment, and Redox Potential Information of Various Cytochrome Species at pH 7.0 and I = 0.19m

species	net charge[d] (e)	dipole magn (Debye)	γ[e] (deg)	$\Delta(\Delta G^{\circ}_{el})$[e] (kcal/mol)	E° [e] (mV)
cytb5	−8.15	597	144		5
hcytc	7.00	327	23		
native ycytc	7.31	485	78	0	290[b]
ycytc K79A	6.35	506	86	−0.046	292[c]
ycytc K'72A	6.32	467	85	+0.138	284[c]
ycytc K79A/K'72A	5.36	497	93	+0.046	288[c]
ycytc R38A	6.39	524	80	+1.176	239[d]

[a] In units of electron charge magnitude. [b] Barker & Mauk, 1992. [c] Guillemette, J. G., et al., in preparation. [d] Komar-Panicucci et al., 1992. [e] γ = angle of dipole moment relative to Fe position vector in the center of mass frame. $\Delta(\Delta G^{\circ}_{el})$ = change in free energy of reduction in kcal/mol relative to native ycytc derived from observed reduction potentials shown in the last column. E° = potential of the reduction half-reaction of wild-type or mutant ycytc determined from cyclic voltammetry experiments.

Mutation Effects on Redox Potential. In addition to estimating the effect of mutations on the diffusion part of the reaction, where electrostatic steering operates, we also incorporated the effect of mutations on the reduction potential of ycytc. The redox potential perturbation effects as determined by cyclic voltammetry experiments (see references in Table II) were included in the total bimolecular kinetic scheme by estimating the effect of changes in the reduction potential on the intrinsic electron-transfer rate constant, k_{et}. Reduction potential changes were manifested as changes in the preexponential term in our model eq 8, and these changes are given by the Marcus equation (Marcus & Sutin, 1985):

$$k_{et}^{\circ} = \upsilon \exp\left[-\frac{(\Delta G_{el}^{\circ} + \lambda)^2}{4\lambda k_B T}\right] \tag{9}$$

where k_{et}° now depends upon redox free energy ΔG_{el}° and reorganization energy λ. We employed the estimate of λ = 0.7 eV for the reorganization energy for the ycytc/cytb5 couple (McLendon & Miller, 1985). With E° of reduction of ycytc equal to 290 mV (Barker & Mauk, 1992) and cytb5 equal to 5 mV, we obtain a value of ΔG_{el}° = −6.57 kcal/mol (or 285 mV) for the wild-type reaction. The factor υ, which is the intrinsic unimolecular electron-transfer rate for juxtaposed heme groups, is still unknown, but it was adjusted to give a match between the theoretical and experimental bimolecular rate constants for the wild-type ycytc/cytb5 reaction. Figure 2 shows the resulting BD bimolecular rate constant varying as a function of k_{et}° at pH 7 and $I = 0.19m$ and using β = 1.0 Å^{-1} for the wild-type ycytc/cytb5 reaction. From this we obtained a best fit value of $k_{et}^{\circ} = 1.3 \times 10^{11}$ s^{-1}, corresponding to $\upsilon = 1.42 \times 10^{12}$ s^{-1}. Then using eq 9, we estimated the k_{et}° value of the mutants using their perturbed ΔG°_{el} values from Table II. The reduction potentials of the mutants are sufficiently close to be potential of the wild-type ycytc that the reduction potential perturbation effect on the rates is minor, except for the R38A mutant where this effect becomes important.

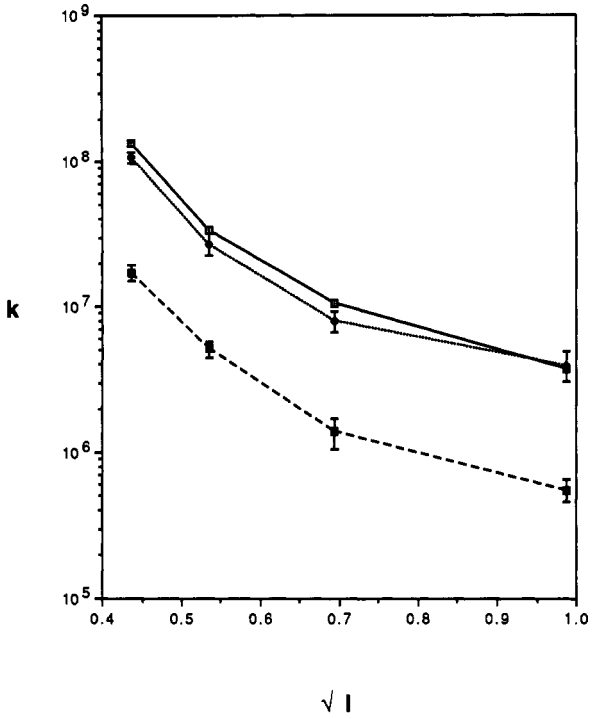

FIGURE 1: Ionic strength dependence of the bimolecular rate constant k for reduction of ycytc by cytb5 at T = 298.15 K and pH 7.0. — is experimental (error bars are smaller than symbol size). Theoretical curves are for the exponential reactivity model with $k_{et}° = 10^{11}$ s^{-1} and distance decay parameters β = 1.2 Å^{-1} (- - -) and β = 1.0 Å^{-1} (···).

Simulations. BD simulations were performed using the program BDTIRM (Brownian Dynamics of two irregular rotating macromolecules), written at Tennessee Technological University, at experimental conditions of pH 7.0, T = 298.15 K, and ionic strengths I = 0.19, 0.286, 0.482, and 0.977m. The R38A mutation was studied at I = 0.163m. These ionic strengths are sufficiently small that electrostatic field effects will still be important, but they are sufficiently large that long-lived electrostatic complexes did not form between the species and drastically slow down the trajectory simulation. Simulations each required approximately 30 h to run on a Personal IRIS.

RESULTS

Ionic Strength Dependence of Variant Cytochrome c Reductions by Cytochrome b_5. As previously observed for the reaction, the second-order rate constants for all of the reactions concerned in the present study are strongly dependent on ionic strength. These rate constants and their uncertainties are set out in Table III.

Optimization of Reaction Parameters. We first discuss the sensitivity of theoretical rates to the choice of intrinsic reaction parameters. Since this is the one part of the BD model that is a "black box", we determined what these parameters should be by matching theoretical rates to experiment. Figure 1 shows the ionic strength dependence of the bimolecular rate constant for reduction of the native ycytc by cytb5, comparing the experimental results with theoretical results using the exponential reactivity model. Here we selected a value for the unknown preexponential factor $k_{et}°$ = 10^{11} s^{-1}, which is of the expected order of magnitude. Simulations were performed for two different values of the spatial decay parameter β. The choice most closely matching

Table III: Second-Order Rate Constants for cytb5 Reduction of ycytc Variants (pH 7.0, 25 °C)

ionic strength (M^{-1})	rate (10^6 M^{-1} s^{-1})	SD
	K'72A Variant	
0.097	180	10
0.19	37	3
0.286	27.6	0.8
0.487	7.6	0.4
0.977	4.0	0.1
1.475	3.3	0.2
	K79A Variant	
0.097	1910	50
0.19	68	3
0.286	32	1
0.487	9.0	0.5
0.977	3.8	0.2
	K'72A/K79A Variant	
0.097	160	10
0.19	30	2
0.286	18	2
0.487	6.1	0.3
0.977	3.2	0.1
1.475	3.2	0.1
	R38A Variant	
0.163	89	9

experiment for this model was β = 1.0 Å^{-1}, and this became our choice for the remainder of the study. The theoretical rate was observed to be a quite sensitive function of β. This value of β is somewhat smaller than the 1.2 Å^{-1} found in our previous study on *P. aeruginosa* c_{551} self-exchange rates, but it is still well within reason on the basis of previous estimates for these types of electron-transfer reactions.

Having chosen a β which gives rates in the correct range, we further refined our parameter estimate by determining a $k_{et}°$ that brings the reaction between wild-type ycytc/cytb5 into agreement with experiment at pH 7 and I = 0.19m, which was our benchmark reaction. A study of the variation of the bimolecular rate constant as a function of the variation of $k_{et}°$ is shown in Figure 2. The rate constant varies nearly linearly with $k_{et}°$ up to about 0.2 ps^{-1}, after which it begins to show saturation behavior. Theory matches experiment for a $k_{et}°$ value of 1.3 × 10^{11} s^{-1}. The choice of parameters β = 1.0 Å^{-1} and $k_{et}°$ = 1.3 × 10^{11} s^{-1} then provided the calibration to the wild-type proteins that we needed to observe the effects of site-directed mutations of charged residues Tml72, Lys79, and Arg38 on ycytc.

Ionic Strength Dependence. Using the exponential reactivity model of $k_{et}(d)$ and our optimized reaction parameters, we performed an ionic strength dependence study of the reaction between the wild-type proteins. The results are shown in Figure 3. Notice that the BD theory with exponential reactivity nicely reproduced the ionic strength dependence found experimentally, indicating (i) a consistent representation of the electrostatic effects on reaction rate, and (ii) a reasonable treatment of the interplay between diffusion and intrinsic electron-transfer dynamics afforded by this model. The same reaction model was studied but instead a uniform dielectric treatment of the medium was used. With a simple Coulomb–Debye treatment of the forces with constant dielectric of 78.3 and a constant ionic strength of 0.19m at all points in space, and with the rate constant nearly matched to experiment at the lowest ionic strength, the dashed curve in Figure 3 demonstrates the failure to reproduce the ionic strength dependence of the reaction when using an inferior treatment of the electrostatics.

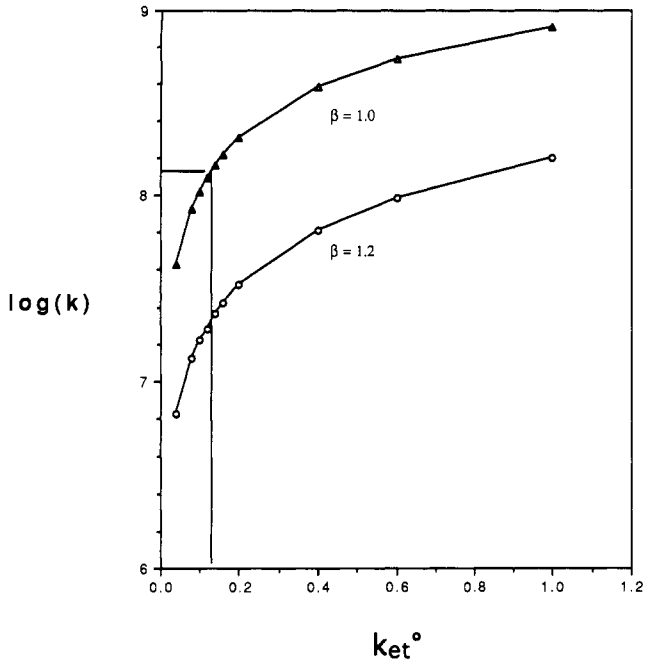

FIGURE 2: Dependence of the theoretical $\log_{10}(k)$ on the choice of exponential reactivity factor $k_{et}°$ for two choices of β (Å^{-1}) for the reduction of ycytc by cytb5 at $I = 0.19m$, pH 7.0, and $T = 298.15$ K. An experimental value for this set of conditions (1.36×10^8 M^{-1} s^{-1}) is used here to choose an appropriate value for $k_{et}°$ ($=1.3 \times 10^{11}$ s^{-1}) for the remainder of these studies.

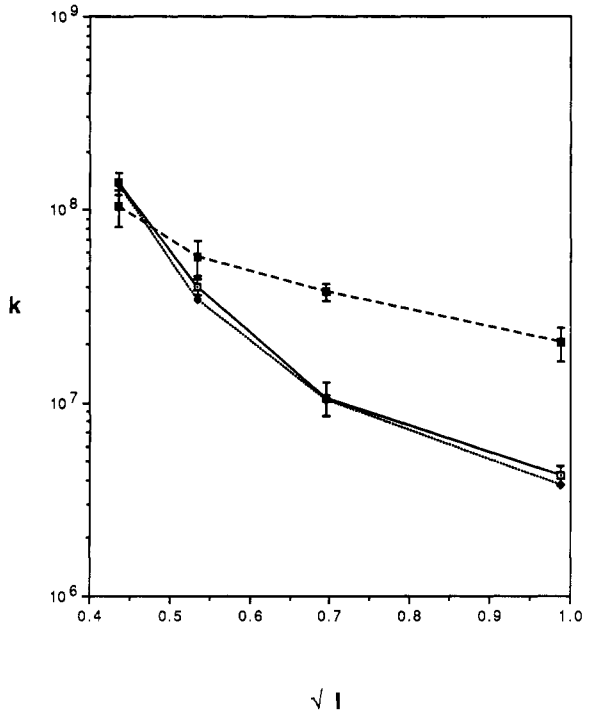

FIGURE 3: Comparison of the rigorous LPB electrostatic model with discontinuous dielectric (···) and the simple Coulomb–Debye uniform dielectric model (- - -) with the experimental (—) bimolecular rate constant as a function of ionic strength at pH 7.0 and $T = 298.15$ K.

Distance Cutoff Model. Figure 4 displays the comparison of experiment to theoretical results using the simple distance cutoff model of reactivity for the reaction of native ycytc with cytb5. The numerical uncertainty using this model is much greater than that using the exponential reactivity model, since the reaction success is either all or nothing for a given trajectory, while for the latter the reaction probability for a

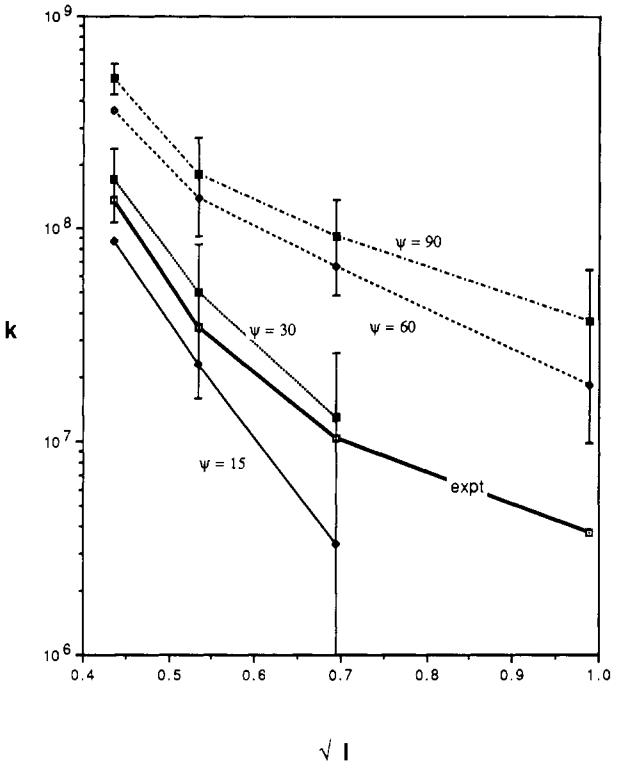

FIGURE 4: Ionic strength dependence of the bimolecular rate constant k for reduction of ycytc by cytb5 at $T = 298.15$ K and pH 7.0. — is experimental (error bars are smaller than the symbol size). Theoretical curves are for the distance cutoff model with $d_{rx} = 12$ Å and four values of the heme plane mutual orientation angle ψ.

single trajectory can be a fractional quantity depending on the residence time in a reactive region of mutual orientation space. The nearest fit to the experiment was obtained using $d_{rx} = 12.0$ Å and a heme coplanarity criterion of $\psi_{rx} = 30.0°$. The minimum value of d_{rx} obtained in the simulation of this reactive pair was 10.3 Å (values less than 11 Å were rarely obtained). Notice that this model does not reproduce the ionic strength dependence of the experiment as well as the exponential reactivity model. Thus, the exponential reactivity model, which takes into account the lifetimes of reactive orientations, does a superior job over a model in which reaction is instantaneous upon reaching certain distances and orientations. This is consistent with a reaction that is not completely diffusion-controlled, but is diffusion-influenced, with the intrinsic electron-transfer unimolecular event entering the dynamics explicitly. This was the conclusion also reached in our previous study of this system using the dipolar sphere model.

BD Analysis of Cytochrome b_5 Reduction of Cytochrome c Variants. We now discuss the results for the treatment of the mutant yeast cytochromes. In Table IV we show the comparison of the theoretical and experimental bimolecular rate constants for the oxidation of cytb5 by ycytc and four mutants at pH 7.0 and $I = 0.19m$. Simulation results for both reaction models are displayed, although for reasons previously stated we were most interested in those generated by the superior exponential reactivity model, with its parameters $\beta = 1.0$ Å^{-1} and $k_{et}°$(wild-type) $= 1.3 \times 10^{11}$ s^{-1} chosen to give the closest fit to the native ycytc/cytb5 reaction. Of the two singly mutated residues Tml72 and Lys79, the greatest retardation of the bimolecular rate was observed with the mutation K'72A. We observed mutation effects both with and without taking into account the mutant effect on the redox potential. In either case the BD simulation correctly repro-

Table IV: Theoretical and Experimental Bimolecular Rate Constants for the Oxidation of cytb5 by ycytc and Four Mutants[a]

species	I (m)	exptl	BD, distance cutoff model[d]	BD,[b] expo model fixed $k_{et}°$	BD,[c] expo driving-force-corrected $k_{et}°$	$k_{et}°$ (ps^{-1})
native ycytc	0.19	136 ± 3	172 ● 63	136 ± 17	136 ± 17	0.130
ycytc K79A	0.19	68 ● 3	62 ± 40	110 ± 10	112 ± 9	0.133
ycytc K′72A	0.19	37 ± 3	55 ± 15	63 ± 3	59 ± 6	0.121
ycytc K79A/K′72A	0.19	30 ± 2	15 ± 23	47 ± 6	46 ● 6	0.127
native ycytc	0.163	290 ± 31	266 ± 49	281 ± 30	281 ± 30	0.130
ycytc R38A	0.163	89	225 ± 77	238 ± 20	126 ± 15	0.069

[a] All rates are given in units of 10^6 M^{-1} s^{-1}. [b] Reaction criterion = exponential reactivity model with $\beta = 1.0$ Å^{-1}, fixed $k_{et}° = 1.3 \times 10^{11}$ s^{-1}. [c] Reaction criterion = exponential reactivity model with $\beta = 1.0$ Å^{-1}, $k_{et}°$ driving-force-corrected, varying according to eq 9. Value of $k_{et}°$ given in last column. [d] Reaction criterion = distance cutoff model with $d_{rx} = 12$ Å, $\psi = 30°$, pH 7.0, $T = 25$ °C.

duced the trend between the wild-type species and the three mutant species, but the quantitative effect on the rate predicted by BD was not quite as large as that found in the experiment. The K′72A mutation was predicted to have a larger effect on the rate than K79A, as also observed experimentally. Inclusion of the perturbation of the redox potential effect (i.e., driving-force-corrected $k_{et}°$) produces only a minor influence since the reduction potential perturbations are so small. The comparison of BD results both with and without the driving-force-corrected $k_{et}°$ is given to show the relative magnitude of perturbing influences of mutations. For instance, the BD rate with *fixed* $k_{et}°$ accounts for how charge mutations affect the distribution of docked conformers through electrostatic steering, while the driving-force-corrected $k_{et}°$ includes the additional influence on the redox potential. Clearly the greatest effect of mutations is manifested in the electrostatics of docking and not changes in the redox potential. The distance cutoff model also predicts the correct trend between mutants at locations 72 and 79, but it predicts an exaggerated quantitative effect on the rate.

The theoretical prediction of rates of reaction of mutant R38A, which is the neutralization of a positive charge outside the exposed heme region of the yeast protein, was also in agreement with experiment. The experiment observed a significant decrease in the bimolecular rate constant caused by this mutation. The BD model excluding the perturbation of reduction potential predicted a slight decrease in the rate, while inclusion of the perturbed reduction potential predicted a decrease comparable to the experiment. The R38A mutation produced a more significant decrease in the reduction potential of ycytc than any of the other variants studied here. Only by inclusion of this retarding effect (by decreasing $k_{et}°$ according to the Marcus eq 9) does BD theory make a correct prediction.

Analysis of Protein–Protein Complexes. We also performed an analysis of protein–protein complexes at points in the BD trajectories where the reaction criteria were most optimally satisfied. During the simulation of bimolecular diffusion-influenced rate constants, for each trajectory which reaches a configuration in which $d < 13$ Å, the coordinates of the most reactive protein–protein configuration of the trajectory were saved on disk. The most reactive configuration was defined as that which achieves the minimum heme–heme distance d within that trajectory, and it was saved on disk as two reference vectors from which we later reconstructed the coordinates of the entire complex. These two vectors are the center of mass position vector of protein II in the reference frame of protein I and a rotational orientation vector for protein II. Thus, the configuration of the complex is a six-dimensional piece of information. The program RECONST was used to reconstruct the full atomic configuration of every saved protein–protein complex from reading the history file of reference vectors. Identifying formally charged atoms only (charge magnitude > 0.4e), an ionic contact list was constructed of the closest 15 contacts. A pairwise interaction energy is also computed, both by a simple uniform dielectric Coulomb–Debye energy term and by a Coulomb–Debye model (CDED) employing an empirical, linearly varying, distance-dependent, effective dielectric constant, ϵ_{eff} (Miller, 1991). This is a two-parameter function given by

$$\epsilon_{eff} = \epsilon_0 + (r/f)(\epsilon_{sol} - \epsilon_0) \qquad r<f \tag{10a}$$

$$\epsilon_{eff} = \epsilon_{sol} \qquad r>f \tag{10b}$$

where r is the charge pair separation distance, ϵ_0 is the inner dielectric constant (4.0), and f is the distance at which the dielectric should return to the solvent dielectric value, ϵ_{sol} = 78.3 (e.g., $f = 30$ Å, approximately the sum of the radii of the two proteins, according to a separate study on proteins of this size).

In Figure 5 we display the incidence of involvement of residues in ionic contacts between proteins in our simulated reactive protein–protein complexes. We tallied the total number of times each formally charged residue appears in the contact list as an indication of the importance of individual residues in forming contacts for productive orientations. This study was performed on the wild-type ycytc/cytb5 reaction at $I = 0.19m$ and pH 7. For cytb5 we found that the negatively charged residues Glu44, Glu48, Glu56, and Asp60 and the most solvent-exposed heme propionate were the groups most frequently involved in protein–protein complexation. This result is expected from the positions of these groups around the heme-exposed face of cytb5, as shown in Figure 7. On the wild-type ycytc, conserved positively charged residues Arg13, Tml72, Lys79, and Lys86 and the most solvent-exposed heme propionate dominated the interactions, again coinciding with the heme-exposed face of ycytc. Notice that the frequency of involvement of ycytc residues in the order Tml72 > Lys79 explains why the K′72A mutation produces the strongest retardation of the rate, followed by K79A. Arg38 was never involved in an ionic contact for any reactive complex we simulated. Its neutralization affects the *global* electrostatic properties of the protein, causing a modest decrease in the rate coupled with a stronger effect on the redox potential, which produces a stronger retarding effect on the rate.

A list of frequency of occurrence of triplets of contacts was also tallied for the 849 complexes generated by BD for the benchmark reaction. Only the closest contact was counted for any given residue within a complex (i.e., a screening procedure was used such that a given atom does not appear twice in the same list for any given complex, but is only listed once with its closest contact shown). The average electrostatic energy of the complex is listed alongside the frequencies of various triplets of contacts in Table V. We list those triplets of contacts which occurred in double digits, along with the

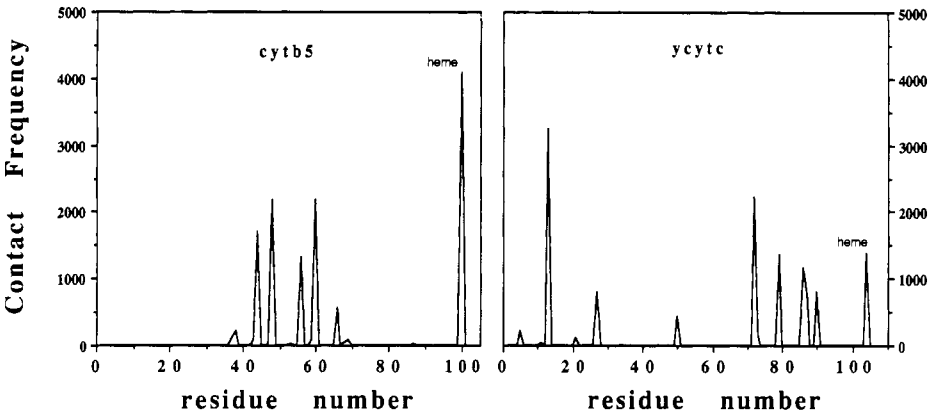

FIGURE 5: Histogram of frequencies at which individual charged residues of ycytc and cytb5 are involved in ionic contacts in 843 reactive complexes generated at $I = 0.19m$, pH 7.0, and $T = 298.15$ K.

Table V: List of Most Frequent Threesomes of Ionic Residue Contacts between cytb5 and Native ycytc from BD Simulations at pH 7, $T = 25$ °C, and $I = 0.19m$[a]

cytb5–ycytc ionic contacts			frequency	energy (kcal/mol)
48–13	60–86	heme–72	65	−13.0 (←)
48–13	56–87	60–86	59	−13.1 (←)
48–13	56–87	heme–72	53	−12.7 (←)
56–87	60–86	heme–72	53	−12.7 (←)
44–27	60–72	heme–79	38	−6.4 (Salemme)
56–87	60–13	heme–72	35	−11.8
48–13	56–86	60–72	24	−13.6
44–5	48–13	60–72	23	−13.1
48–27	60–13	heme–72	21	−7.1
44–86	48–72	heme–13	20	−9.6
44–27	56–87	heme–72	19	−10.4
44–87	60–72	heme–13	19	−8.4
44–5	48–13	56–86	18	−12.7
44–13	48–86	60–72	18	−9.6
48–13	60–72	heme–79	18	−6.3 (Salemme)
48–27	60–72	heme–79	18	−5.9
44–13	48–72	60–79	17	−6.6
44–27	56–87	60–13	16	−10.2
56–13	60–72	heme–79	16	−6.0
44–87	48–86	60–72	15	−10.4
44–87	48–86	heme–13	15	−9.8
44–27	60–86	heme–72	14	−10.5
44–5	56–86	60–72	14	−12.9
44–79	48–27	heme–72	14	−5.7
44–5	48–87	heme–13	13	−7.8
44–27	48–13	60–86	13	−10.9
44–27	48–13	heme–72	13	−10.9
44–72	60–27	heme–13	13	−7.6
44–86	60–72	heme–13	13	−7.9
48–86	60–72	heme–13	13	−9.8
44–27	48–13	60–72	12	−6.4 (Salemme)
44–13	48–72	heme–27	11	−5.7
44–27	48–13	heme–79	11	−6.3 (Salemme)
44–72	48–79	60–27	11	−6.9
44–27	60–13	heme–72	11	−8.8
48–27	56–13	60–72	11	−6.4
48–72	60–79	heme–27	11	−5.6
60–87	66–72	heme–13	11	−9.7
48–27	56–13	heme–79	10	−5.9
44–27	48–13	56–87	10	−10.8
44–27	56–87	60–86	10	−10.8
44–72	48–79	heme–13	10	−6.9
44–79	60–13	heme–72	10	−6.1
44–86	48–72	60–79	10	−8.4

[a] Salemme and Rodgers et al. type complexes are indicated, along with a more frequent and stable complex type indicated by arrows. Average energy of the complexes was computed using a distance-dependent effective dielectric function, eq 10.

average electrostatic interaction energy for the different contact types. Those of the Salemme (1976) and Rodgers et al. (1988) type are indicated, while an even more dominant and electrostatically favorable type of interaction we discovered is indicated by the arrows. From a composite of this table, we found a predominance of two types of complexes. The most predominant involves the quartet of interactions Glu48–Arg13, Glu56–Lys87, Asp60–Lys86, and heme–Tml72 (cytb5 residues listed first). These had an average electrostatic energy of −13.0 kcal/mol, using the CDED model eq 10. The second most important type of complexes was of the Salemme and Rodgers et al. type, with interactions Glu44–Lys27, Glu48–Arg13, Asp60–Tml72, and heme–Lys79 and having an average interaction energy of −6.4 kcal/mol. These complexes were formed by rigid body docking in the BD algorithm, and so do not reflect additional stabilization from side-chain rotations. In Figure 6a,b we depict a stereo rendering of a representative from each of these two complex types. The Salemme model (Figure 6b) is able to achieve essentially coplanar hemes, while the other complex type does not. The representative in Figure 6a exhibits a mutual heme plane angle of 17°, but is more electrostatically stable than the complexes described previously. A number of other minor types of complexes were also observed, indicating not a single type of stable reactive protein–protein complex but a spectrum of structurally similar suboptimal complexes.

In Figure 7 we present what we call a "docking profile" for the cytb5 molecule. For each reactive complex we placed a point representing the center of mass of the incoming ycytc relative to cytb5. We observed that all points were in the region of the exposed heme edge on cytb5, the most dense region being at the top of the diagram, where both our predominant type and the Salemme types occur. These complexes thus differ essentially by a rotational orientation around the protein–protein axis. A scattering of points away from this dominant region also occurred. This profile is unlike that observed previously for cytochrome *c* and cytochrome *c* peroxidase, where two or more widely disparate regions of reactive approach around the peroxidase enzyme were observed.

Recent work (Rodgers & Sligar, 1991) mapped the electrostatic interactions between these two proteins by measuring volume changes due to high-pressure disruption of complexes together with site-directed mutagenesis. This technique allowed the assessment of the importance of individual charged residues in the protein–protein complexes. Their results seem to implicate one major orientation of the complex at neutral pH, rather than sampling of multiple orientations on the surface, as our study suggests. Furthermore, the complex described by Rodgers and Sligar appears to involve the four ionic contacts consistent with the Salemme

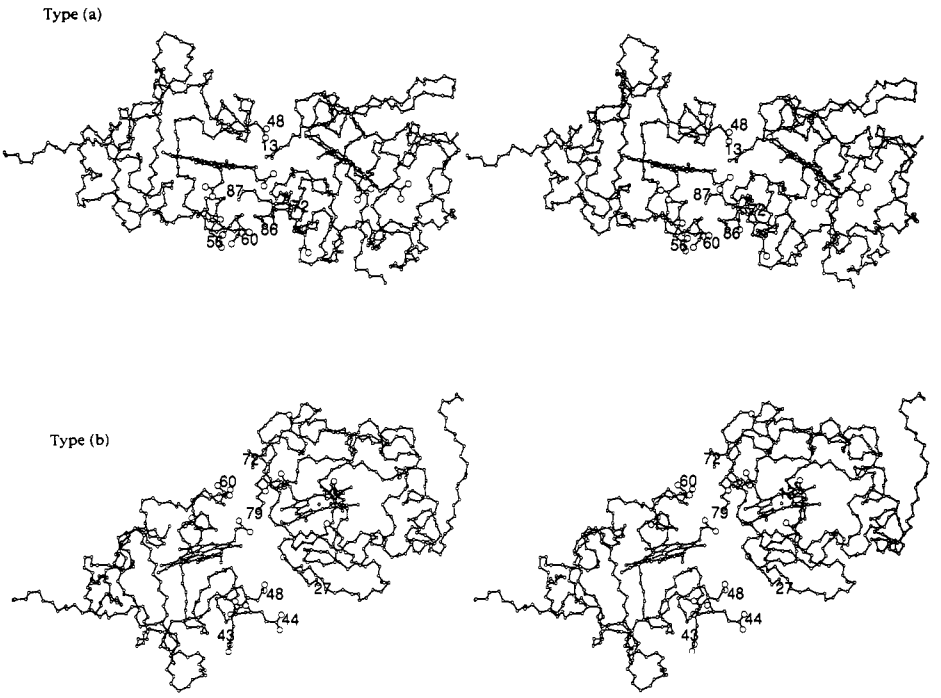

FIGURE 6: Stereographic projection of representatives from two predominant types of reactive docked complexes between cytb5 and ycytc generated in BD simulation at $I = 0.19m$, pH 7.0, and $T = 298.15$ K. Type a is the most frequent and electrostatically stable type of complex observed; type b is similar to the Salemme model-built complex, which is the next most frequently observed type. Protein cytb5 is on the left.

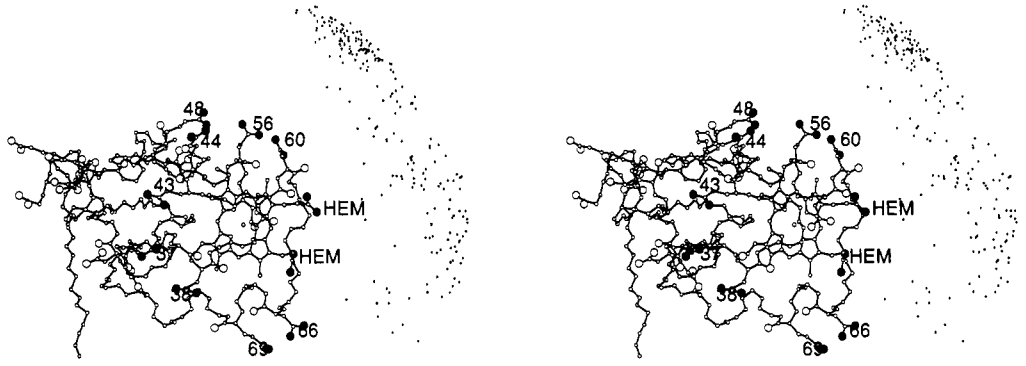

FIGURE 7: Docking profile showing target protein cytb5 surrounded by dots which represent the center of mass of an incoming ycytc molecule in reactive docked complexes at $T = 298.15$ K and pH 7.0.

model. However, their study was performed at low ionic strength (2 mM Tris-HCl), where electrostatic forces are much stronger and are likely to help lock the complex into a single orientation. Besides, their technique observes equilibrium properties of the complexes, while our simulation (and the bimolecular kinetics) reflects short-lived dynamical behavior involved in electron transfer from suboptimal complexes.

CONCLUSIONS

This study represents the first investigation of the effects of cytochrome *c* surface mutations on the bimolecular kinetics of electron transfer with another electron-transfer protein. As the effects of these protein modifications on the rate constants determined in this work are subtle in nature, detailed mechanistic interpretation of these results is virtually impossible without the assistance of relatively sophisticated modeling procedures. For this reason, this study has employed the most advanced and rigorous Brownian dynamics simulation procedure available for the calculation of diffusional docking trajectories between two whole translating and rotating proteins. The diffusion algorithm was coupled to a realistic model of the chemical reaction event embodied in an intrinsic electron-transfer unimolecular rate constant which varies exponentially with heme–heme distance. Proteins were treated as topologically irregular rigid bodies according to their X-ray crystallographic structures. Electrostatic interactions were calculated by finite difference iteration of the linearized Poisson–Boltzmann equation. By comparison with biomolecular rate constants obtained experimentally for reaction of the wild-type and mutant cytochromes, we have demonstrated that the BD simulation method is able to predict bimolecular rate constants quantitatively for the electron-transfer reaction of these cytochromes over a considerable range of ionic strengths. Quantitative agreement was made possible only by using the exponential electron-transfer model and by suitable adjustment of reactivity parameters. These parameters include the distance decay parameter β, which was theoretically determined for this reaction pair to have a value of 1.0 $Å^{-1}$. This value is in reasonable agreement with estimates made for these types of systems.

We also explored a primitive distance cutoff model of the reaction event in which the reaction was assumed to occur instantaneously upon attainment of specific heme–heme interatomic distances and mutual heme planar angles. The

reaction in such a model is assumed to be completely diffusion-controlled. The exponential reactivity model gives results that are more precise and more accurate than those provided by the simpler distance cutoff model. Thus, the exponential reactivity model, which takes into account the lifetimes of reactive orientations, did a superior job over a model in which reaction is instantaneous upon reaching certain distances and orientations. This result is consistent with a reaction that is not completely diffusion-controlled but is diffusion-influenced, with the intrinsic electron-transfer unimolecular event explicitly entering the dynamics.

The advanced treatment of the electrostatic fields around the proteins is essential to the quantitative agreement with experiment. For example, the ionic strength dependence of the bimolecular reaction rate was well reproduced by the most advanced dielectric model, which takes into account the dielectric discontinuity between the interior and exterior of the proteins, but it is poorly reproduced by the uniform dielectric model.

We also determined the effects of selective charge site perturbations by mutating residues Tml72 and Lys79 on the heme-exposed face of ycytc and Arg38 on the opposite face into neutral alanine residues. The trends in the rates of the various mutants of ycytc were well reproduced by the simulations for all of the mutations studied: K79A, K′72A, K79A/K′72A, and R38A. The experimentally observed rate constants descend in the following order (at $I = 0.19m$): native ycytc > K79A > K′72A > K79A/K′72A; the R38A mutant (studied at $I = 0.163m$) also reacts more slowly than the wild type. Thus, all mutants react more slowly than the wild-type protein.

We also incorporated the observed influence of mutations on the reduction potential of ycytc. Using Marcus theory and an estimated reorganization energy, we estimated the perturbation in the intrinsic electron-transfer rate constant caused by the charge mutations. Inclusion of this effect in the BD simulations did not change the predicted trend and had a minor numerical effect on the K79A, K′72A, and K79A/K′72A series. Inclusion of this effect was important for the R38A mutation.

By generating docking profiles in the simulations, we observed that these proteins approach one another for efficacious electron transfer through essentially a single domain. The distance of closest approach of the two heme groups in rigid body docking is typically around 12 Å, with heme planar angle mutual orientations able to take on a wide range of values at this distance. Further energy minimization optimization or molecular dynamics of these complexes would no doubt yield smaller, more realistic heme–heme distances (Wendoloski et al., 1987). Our previous study of docking of horse heart cytochrome *c* with yeast cytochrome *c* peroxidase (Northrup et al., 1987, 1988) revealed two or more distinct domains of docking association satisfying fairly stringent geometric criteria for electron transfer. These were necessarily invoked to account for the large bimolecular rates. On the surface this seems to be contradicted by an exciting new finding by Pelletier and Kraut (1992) that cytochrome *c*/cytochrome *c* peroxidase binds in a single highly specific complex in the crystal. However, such binding in the crystal, an equilibrium phenomenon, does not necessarily preclude the existence of a spectrum of suboptimal complexes in solution which contribute to electron transfer. Furthermore, the conditions of crystallization are quite different than the physiological ionic strength environment of the kinetic studies we have been simulating. For the present reaction, we do in fact predict a single binding domain contributing to electron-transfer bimolecular dynamics, but not a single conformation as would be observed in a stable crystal. We have demonstrated in simulations of more generic protein–protein systems (Northrup & Erickson, 1992) that the bimolecular rate of attaining a single protein–protein conformation with total loss of orientational degrees of freedom would be exceedingly slow, much slower in fact than the observed rate constants for either the cytc/ccp reaction or the reaction studied here.

By examining the ionic contacts formed in our BD-simulated complexes, we observed two predominant classes of 1:1 complexes. The most predominant involves the quartet of interactions Glu48–Arg13, Glu56–Lys87, Asp60–Lys86, and heme–Tml72 (cytb5 residues listed first). These had an average electrostatic energy of −13.0 kcal/mol. The second most important type of complexes was the Salemme and Rodgers et al. type with interactions Glu44–Lys27, Glu48–Arg13, Asp60–Tml72, and heme–Lys79 and having a smaller average interaction energy of −6.4 kcal/mol. Other complexes were also observed which were rotational variants of these. These results are in agreement with a recent NMR characterization (Burch et al., 1990) of complexes in solution, which indicated the involvement of at least six lysyl residues, two more than predicted by static model building and implicating two or more structurally similar 1:1 complexes in solution. A previous study of this reaction also postulated an ensemble of protein–protein complexes in solution as precursors to an efficient electron-transfer geometry (Mauk et al., 1986).

Clearly there are some limitations to the present simulation method which need to be addressed in future work. The rigid body docking of two proteins is probably inadequate to capture the true dynamics of protein–protein association. Our method is perhaps best suited to generate loosely docked complexes which should be further refined through molecular dynamics. However, we must hasten to add that our preliminary simulation on the cytc/ccp system employing dynamic surface side chains does not appear to change qualitatively the results we have obtained for that system. The second most obvious deficiency of our current model is the exponential reaction criterion. We do not mean to imply a through-space model of electron transfer by using this theory, but simply use the exponential function and parameters to specify the "hotness" of the protein surface toward electron transfer and to allow a dynamical coupling between diffusion and reaction events. The utility of the BD method for computation of electron-transfer rates between metalloproteins will increase as more detailed modeling of the intrinsic electron-transfer step is incorporated. Since the simple exponential distance decay model is probably inadequate, the parameters λ and β should be viewed as effective quantities useful for correlating the behavior of a wide range of kinetic data. A more complete knowledge of the variable reactivity of the protein surfaces is being made available by analysis of bonding pathways (Beratan et al., 1992), and these theories could be included in our modeling by special reactivity functions.

ACKNOWLEDGMENT

We thank Dr. James B. Matthew for providing the Tanford–Kirkwood computer program, Dr. F. Scott Mathews for communication of cytb5 coordinates, and Dr. Gary Brayer for an advanced copy of the ycytc coordinates. S.H.N. thanks Christine Northrup for secretarial support and encouragement.

REFERENCES

Andrew, S. M., Thomasson, K. A., & Northrup, S. H. (1993) *J. Am. Chem. Soc.* (in press).

Barker, P. D., & Mauk, A. G. (1992) *J. Am. Chem. Soc. 114*, 3619.

Beratan, D. N., Betts, J. N., & Onuchic, J. N. (1992) *J. Phys. Chem. 96*, 2852.

Bernstein, T. C., Koetzle, T. F., Williams, G. J. B., Meyer, E. J., Jr., Brice, M. D., Rodgers, J. R., Kennard, O., Shimanouchi, T., & Tasumi, M. (1977) *J. Mol. Biol. 112*, 535.

Burch, A. M., Rigby, S. E. J., Funk, W. D., MacGillivray, R. T. A., Mauk, M. R., Mauk, A. G., & Moore, G. R. (1990) *Science 247*, 831.

Bushnell, G., Louie, G. V., & Brayer, G. D. (1990) *J. Mol. Biol. 214*, 585.

Dixon, D. W., Hong, X., & Woehler, S. E. (1989) *Biophys. J. 56*, 339.

Dixon, D. W., Hong, X., Woehler, S. E., Mauk, A. G., & Sishta, B. P. (1990) *J. Am. Chem. Soc. 112*, 1082.

Durley, R. C. E., Mathews, F. S., private communication.

Eltis, L. D. (1990) Ph.D. Dissertation, University of British Columbia, Vancouver, BC, Canada.

Eltis, L. D., Herbert, R. G., Barker, P. D., Mauk, A. G., & Northrup, S. H. (1991) *Biochemistry 30*, 3663.

Ermak, D. L., & McCammon, J. A. (1978) *J. Chem. Phys. 69*, 1352.

Funk, W. D., Lo, T. P., Mauk, M. R., Brayer, G. D., MacGillivray, R. T. A. M., & Mauk, A. G. (1990) *Biochemistry 29*, 5500.

Gray, H. B. (1986) *Chem. Soc. Rev. 15*, 17.

Guillemette, J. G., Inglis, S. C., Smith, M., & Mauk, A. G., in preparation.

Hazzard, J. T., Poulos, T. L., & Tollin, G. (1987) *Biochemistry 26*, 2836.

Herbert, R. G., & Northrup, S. H. (1989) *J. Mol. Liq. 41*, 207.

Hoffman, B. M., & Ratner, M. A. (1987) *J. Am. Chem. Soc. 109*, 604.

Inglis, S. C., Guillemette, J. G., Johnson, J. A., & Smith, M. (1991) *Protein Eng. 4*, 569.

King, G. C., Binstead, R. A., & Wright, P. E. (1985) *Biochim. Biophys. Acta 806*, 262.

Klapper, I., Hagstrom, R., Fine, R., Sharp, K., & Honig, B. (1986) *Proteins 1*, 47.

Komar-Panicucci, S., Bixler, J., Bakker, G., Sherman, F., & McLendon, G. (1992) *J. Am. Chem. Soc. 114*, 5443.

Leung, P. S. K., Betterton, E. A., & Hoffman, M. R. (1989) *J. Phys. Chem. 93*, 430.

Marcus, R. A., & Sutin, N. (1985) *Biochim. Biophys. Acta 811*, 265.

Mathews, F. S., Levine, M., & Argos, P. (1972) *J. Mol. Biol. 64*, 449.

Mathews, F. S., & Czerwinski, E. W. (1986) in *Enzymes of Biological Membranes*, 2nd ed. (Martonosi, A. N., Ed.) Vol. 4, p 235, Plenum, New York.

Matthew, J. B. (1985) *Annu. Rev. Biophys. Biophys. Chem. 14*, 387.

Mauk, A. G., Coyle, C. L., Bordignon, E., & Gray, H. B. (1979) *J. Am. Chem. Soc. 101*, 5054.

Mauk, M. R., Mauk, A. G., Weber, P. C., & Matthew, J. B. (1986) *Biochemistry 26*, 7085.

Mayo, S. L., Ellis, W. R., Crutchley, R. J., Jr., & Gray, H. B. (1986) *Science 233*, 948.

McLendon, G. L. (1988) *Acc. Chem. Res. 21*, 160.

McLendon, G. L., & Miller, J. R. (1985) *J. Am. Chem. Soc. 107*, 7811.

Miller, C. (1991) M.S. Thesis, Tennessee Technological University, Cookeville, TN.

Nambi, P., Wierzbicki, A., & Allison, S. A. (1991) *J. Phys. Chem. 95*, 9595.

Northrup, S. H., & Herbert, R. G. (1990) *Int. J. Quant. Chem.: Quant. Biol. Symp. 17*, 55.

Northrup, S. H., & Erickson, H. P. (1992) *Proc. Natl. Acad. Sci. U.S.A. 89*, 3338.

Northrup, S. H., Pear, M. R., Morgan, J. D., McCammon, J. A., & Karplus, M. (1981) *J. Mol. Biol. 153*, 1087.

Northrup, S. H., Allison, S. A., & McCammon, J. A. (1984) *J. Chem. Phys. 80*, 1517.

Northrup, S. H., Reynolds, J. C. L., Miller, C. M., Forrest, K. J., & Boles, J. O. (1986) *J. Am. Chem. Soc. 108*, 8162.

Northrup, S. H., Boles, J. O., & Reynolds, J. C. L. (1987a) *J. Phys. Chem. 91*, 5991.

Northrup, S. H., Luton, J. A., Boles, J. O., & Reynolds, J. C. L. (1987b) *J. Comput.-Aided Mol. Des. 1*, 291.

Northrup, S. H., Boles, J. O., & Reynolds, J. C. L. (1988) *Science 241*, 67.

Pelletier, H., & Kraut, J. (1992) *Science 258*, 1748.

Pielak, G. J., Mauk, A. G., & Smith, M. (1985) *Nature 313*, 152.

Rafferty, S. P., Pearce, L. L., Barker, P. D., Guillemette, J. G., Kay, C. M., Smith, M., & Mauk, A. G. (1990) *Biochemistry 29*, 9365.

Rodgers, K. K., & Sligar, S. G. (1991) *J. Am. Chem. Soc. 113*, 9419.

Rodgers, K. K., Pochapsky, T. C., & Sligar, S. G. (1988) *Science 240*, 1657.

Salemme, F. R. (1976) *J. Mol. Biol. 102*, 563.

Shire, S. J., Hanania, G. I. H., & Gurd, F. R. N. (1974) *Biochemistry 13*, 2967.

Siders, P., Cave, R. J., & Marcus, R. A. (1984) *J. Chem. Phys. 81*, 5613.

Summers, F. E., & Erman, J. E. (1988) *J. Biol. Chem. 263*, 14267.

Tanford, C., & Kirkwood, J. G. (1957) *J. Am. Chem. Soc. 79*, 5333.

Tanford, C., & Roxby, R. (1972) *Biochemistry 11*, 2192.

Timkovich, R., Cai, M. L., & Dixon, D. W. (1988) *Biochem. Biophys. Res. Commun. 150*, 1044.

von Bodman, S. B., Schuler, M. A., Jollie, D. R., & Sligar, S. G. (1986) *Proc. Natl. Acad. Sci. U.S.A. 83*, 9443.

Warwicker, J., & Watson, H. C. (1982) *J. Mol. Biol. 157*, 671.

Wendoloski, J. J., Matthew, J. B., Weber, P. C., & Salemme, F. R. (1987) *Science 238*, 794.